

# Optimal Placement and Sizing of Distributed Battery Storage in Low Voltage Grids for Receding Horizon Control Strategies

Philipp Fortenbacher, Andreas Ulbig, and Göran Andersson

**Abstract**—In this paper we present a novel methodology to leverage model predictive control (MPC) strategies for distributed battery storage in a planning problem using a Benders decomposition technique. The objective of the MPC strategy is to maximize the photovoltaic (PV) utilization and minimize battery degradation of a local residential area, while satisfying the grid constraints. Through a case study we solve an optimal placement and sizing problem for different control strategies with different prediction horizons. For the CIGRE low voltage (LV) benchmark grid, we show that the economic merit of MPC based storage control strategies is superior as compared with heuristic storage control strategies, because they exploit the value of forecast information. The merit can be further increased by incorporating a battery degradation model in the MPC strategy.

**Keywords**—power systems, predictive control, energy storage

## I. INTRODUCTION

Energy storage technologies are believed to play a key role in future to decarbonize the power sector [1]. In particular, battery storage can increase the economic value [2], since battery costs are falling rapidly [3]. Through the expansion of Renewable Energy Sources (RES), the power system integrates more and more Distributed Generation (DG) sources such as photovoltaic (PV) generators [4]. Since a large amount of PV generators is installed in Low Voltage (LV) grids and the grid capacity is limited, it can be expected that system operators will suffer from grid congestions. In this context, Distributed Battery Storage (DBS) configurations can help Distribution System Operators (DSOs) to mitigate grid congestions at high PV penetration levels that are present in LV grids. But DBS installations in combination with PV are also able to increase the PV self-consumption and thus lower the electricity costs for end-consumers.

A lot of research has been done to evaluate operational storage control strategies in terms of their profit [5], [6]. In such studies the size and location of the storage devices are either fixed and placed according to best practice methods or modeled as one centralized or aggregated storage unit. However, especially for DBS applications, the size and location of the battery systems greatly affects the Return on Investment (ROI), such that these studies do not give optimal results.

To overcome this issue, one has to combine planning considerations with operational aspects. Some recent papers propose sizing and placement strategies that involve infinite

prediction horizons [7]–[9]. However, considering such long horizons does not reflect the operational strategy, since, in reality, predictive dispatch methods can only act on shorter horizons e.g. in the presence of predictive Receding Horizon Control (RHC) strategies. This is due to the fact that accurate weather and load predictions are only available for periods on a weekly base.

Another way to tackle such problems is to search for the optimal storage location and size in the parameter space. This is reported in [10], [11] for non-predictive heuristic storage control strategies. However, it can be foreseen that such brute force methods are intractable when longer prediction horizons or a high number of storage devices are involved.

The main objective of this paper is to develop a planning strategy that leverages Model Predictive Control (MPC) control strategies acting on different prediction horizons to find the optimal location and size of DBS. The objective of the underlying MPC strategy is to maximize the PV utilization, while taking battery degradation into account and complying with grid constraints of a local residential area.

The contribution of this paper is the development of a Benders decomposition algorithm for DBS applications that links the operational domain with the planning domain. In our previous work [12] we developed a linearized Optimal Power Flow (OPF) scheme for LV grids and incorporated the resulting Linear Programming (LP) problem in a multi-period OPF problem to solve an optimal placement and sizing problem for an infinite prediction horizon. As an extension we incorporate our linearized OPF scheme into an MPC control strategy that reflects the operational strategy. The linear MPC strategy allows to decompose the multi-period OPF problem into smaller subproblems by applying a Benders decomposition technique [13]. Unlike [14] the subproblems cannot be solved in a parallel fashion, since storage induces a coupling between the subproblems. Nevertheless, we show how we can formulate a Benders decomposition algorithm for this problem class.

The remainder of this paper is organized as follows. Section II defines the problem that we aim to solve. Section III reviews the optimal placement and sizing problem and describes the proposed Benders decomposition method. Section IV presents the simulation results and an economic assessment. Finally, Section V presents the conclusions.

P. Fortenbacher, A. Ulbig, and G. Andersson are with the Power Systems Laboratory, ETH Zurich, Switzerland (e-mail: {fortenbacher, ulbig, andersson}@eeh.ee.ethz.ch).

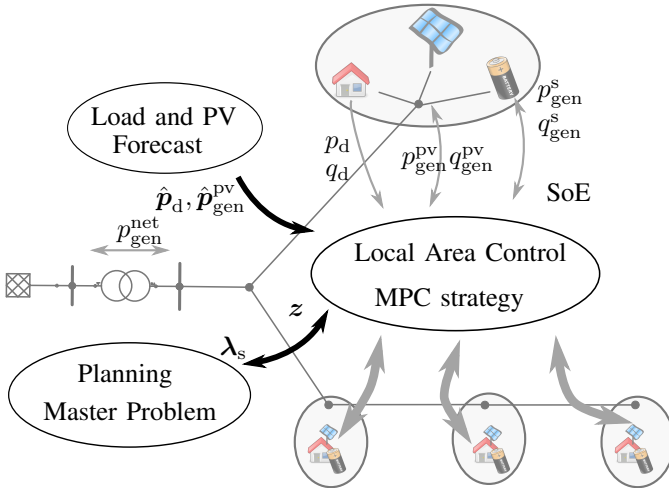


Figure 1. Illustration of the test case environment. The overall objective of the proposed MPC strategy is to maximize PV utilization and to minimize battery degradation. Dual variables and decision variables are exchanged between planning master problem and MPC storage control strategy.

## II. PROBLEM DEFINITION

Figure 1 illustrates the test case environment. We assume that we have a residential local area with high PV penetration and installed storage devices, which are determined with the energy capacities  $z$  by the planning master problem. The area has a centralized local area control entity and has a communication infrastructure. The storage control entity acts as a scheduler with prediction horizons ranging from 24 hours-1 month and is an MPC controller that incorporates a multi-period distribution-level OPF. By using an OPF method, we enable the optimal utilization of the grid and make use of optimal Active Power Curtailment (APC) and Reactive Power Control (RPC). We solve a multi-period problem considering a two-tariff price scenario and a feed-in tariff for the net power  $p_{gen}^{net}$ . In this way, we impose that the scheduler exploits the price differences from the tariff scheme and maximizes the PV self-consumption of the local area. In addition, we incorporate an additional battery degradation objective to assess when revenue benefits outweigh degradation cost. The MPC controller gets perfect load  $\hat{p}_d$  and solar  $\hat{p}_{gen}^{pv}$  forecast time-series and schedules the control inputs of the real and reactive powers for the batteries  $p_{gen}^s, q_{gen}^s$  and the PV generators  $p_{gen}^{pv}, q_{gen}^{pv}$ . It has also the knowledge of the State of Energy (SoE) of the batteries acting as a feedback signal to run a new optimization cycle. To account for energy, the SoE definition is needed. It differs from the State of Charge (SoC) due to the nonlinear relationship between open-circuit potential and charge. The dual variables  $\lambda_s$  need to be exchanged with the planning problem to initiate a new iteration of the Benders decomposition.

### III. OPTIMAL PLACEMENT AND SIZING PROBLEM

#### A. Single shot linearized OPF Problem

We extend our OPF method from [12] to incorporate any convex generator cost functions. For the sake of convenience, we state the optimization problem in a more compact form. We first define the optimization vector  $x =$

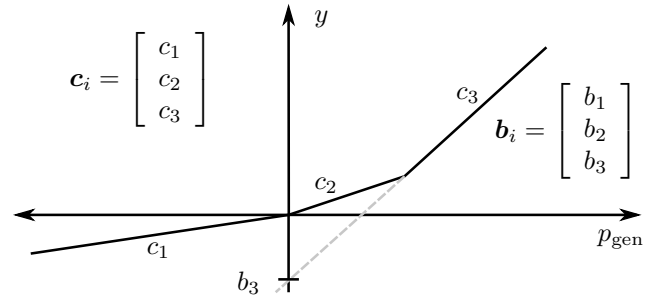


Figure 2. Piecewise-affine (PWA) cost function representation showing illustratively three line segments to reflect any convex generator cost curves.

$[p_1^p, p_1^q, p_{gen}, q_{gen}, v]^T$  reflecting all grid related variables. The active and reactive  $n_g$  generator bus injections  $p_{gen} \in \mathbb{R}^{n_g \times 1}$  and  $q_{gen} \in \mathbb{R}^{n_g \times 1}$  are mapped to  $n_b$  buses with the matrix  $C_g \in \mathbb{R}^{n_b \times n_g}$ . The power line loss vectors  $p_1^p \in \mathbb{R}^{n_l \times 1}$  and  $p_1^q \in \mathbb{R}^{n_l \times 1}$  are associated with the active and reactive power losses of the  $n_l$  lines. The vector  $v \in \mathbb{R}^{n_b \times 1}$  denotes the bus voltage magnitudes. The extended linearized optimization problem is then:

$$\begin{aligned}
 J^* = \min_{x, y} & \quad \mathbf{1}^T y \\
 \text{s.t.} & \\
 \text{(a)} & \quad A_{\text{cost}}^x x - A_{\text{cost}}^y y \leq -b_{\text{cost}} \\
 \text{(b)} & \quad A_g^{\text{in}} x \geq b_g^{\text{in}} \\
 \text{(c)} & \quad A_g^{\text{eq}} x = b_g^{\text{eq}} \\
 \text{(d)} & \quad x_{\min} \leq x \leq x_{\max} \quad ,
 \end{aligned} \tag{1}$$

where  $y \in \mathbb{R}^{n_g \times 1}$  specifies the generator costs. Constraint set (1a) specifies piecewise-affine (PWA) generator cost functions. The matrices and vectors in (1a) are specified as follows

$$\begin{aligned}
 A_{\text{cost}}^x &= [\mathbf{0} \ \mathbf{0} \mid \text{blkdiag}\{c_1, \dots, c_{n_g}\} \mid \mathbf{0} \ \mathbf{0}] \\
 A_{\text{cost}}^y &= \text{blkdiag}\{\mathbf{1}, \dots, \mathbf{1}\} \quad b_{\text{cost}} = [b_1, \dots, b_{n_g}]^T, \tag{2}
 \end{aligned}$$

where  $c_i \in \mathbb{R}^{n_{is} \times 1}$  and  $b_i \in \mathbb{R}^{n_{is} \times 1}$  assign the gradients and offsets of the PWA cost function for each generator. The variable  $n_{is}$  specifies the number of the cost function segments. Figure 2 illustrates the PWA cost function representation for three line segments and one generator.

The grid related constraints (1b,c) incorporate the power balance condition, voltage, loss and line power flow approximations. We define

$$A_g^{\text{in}} = \begin{bmatrix} I & \mathbf{0} & -L_1 C_g & \mathbf{0} & \mathbf{0} \\ I & \mathbf{0} & L_1 C_g & \mathbf{0} & \mathbf{0} \\ I & \mathbf{0} & -L_0 C_g & \mathbf{0} & \mathbf{0} \\ I & \mathbf{0} & L_0 C_g & \mathbf{0} & \mathbf{0} \\ \mathbf{0} & I & \mathbf{0} & -L_1 C_g & \mathbf{0} \\ \mathbf{0} & I & \mathbf{0} & L_1 C_g & \mathbf{0} \\ \mathbf{0} & I & \mathbf{0} & -L_0 C_g & \mathbf{0} \\ \mathbf{0} & I & \mathbf{0} & L_0 C_g & \mathbf{0} \\ \mathbf{0} & \mathbf{0} & B_r C_g & \mathbf{0} & \mathbf{0} \\ \mathbf{0} & \mathbf{0} & -B_r C_g & \mathbf{0} & \mathbf{0} \end{bmatrix} \quad b_g^{\text{in}} = \begin{bmatrix} -L_1 p_d \\ L_1 p_d \\ -L_0 p_d \\ L_0 p_d \\ -L_1 q_d \\ L_1 q_d \\ -L_0 q_d \\ L_0 q_d \\ -i_b^{\text{max}} + B_r p_d \\ i_b^{\text{max}} - B_r p_d \end{bmatrix} \tag{3}$$

$$A_g^{\text{eq}} = \left[ \begin{array}{cc|c|c|c} -\mathbf{1}^T & -\mathbf{1}^T & \mathbf{1}^T & \mathbf{0} & \mathbf{0} \\ \mathbf{0} & \mathbf{0} & B_v \begin{bmatrix} C_g \\ \mathbf{0} \end{bmatrix} & B_v \begin{bmatrix} \mathbf{0} \\ C_g \end{bmatrix} & -I \end{array} \right]$$

$$\mathbf{b}_g^{\text{eq}} = \begin{bmatrix} -\mathbf{1}^T \mathbf{p}_d \\ \mathbf{B}_v \begin{bmatrix} \mathbf{p}_d \\ \mathbf{q}_d \end{bmatrix} - \mathbf{1} \end{bmatrix}, \quad (4)$$

where  $\mathbf{L}_0, \mathbf{L}_1, \mathbf{B}_r, \mathbf{B}_v$  are specified in [12]. In particular,  $\mathbf{L}_0, \mathbf{L}_1$  are hyperplanes describing the losses with inner approximations,  $\mathbf{B}_r$  maps the nodal injections to the branch flows, and  $\mathbf{B}_v$  linearly approximates the bus voltages as a function of the bus injections in active and reactive power. The vector  $\mathbf{i}_b^{\text{max}} \in \mathbb{R}^{n_l \times 1}$  corresponds to the line current limits representing thermal line limits. The vectors  $\mathbf{p}_d, \mathbf{q}_d \in \mathbb{R}^{n_b \times 1}$  specify the nodal load consumption in real and reactive power. Constraint (1d) specifies lower and upper bounds for voltages and active and reactive generator powers. We can also define circular-bounded and power factor based {P,Q} operating areas as reported in [15].

### B. Multi-period Problem

The placement and sizing problem can be formulated as a multi-period problem over a given prediction horizon  $N$ . Its purpose is to find the optimal placement and sizes of storage devices, while considering a certain operational strategy. We introduce a further optimization vector  $\mathbf{z} \in \mathbb{R}^{n_s \times 1}$  that specifies the energy capacities of  $n_s$  batteries. We extend  $\mathbf{X} = [\mathbf{x}_1, \dots, \mathbf{x}_N]^T$  and  $\mathbf{Y} = [\mathbf{y}_1, \dots, \mathbf{y}_N]^T$  to account for multiple steps. The placement problem from [12] can be written as follows in a more compact form:

$$J^* = \min_{\mathbf{X}, \mathbf{Y}, \mathbf{z}, \mathbf{D}} T \underbrace{\left( \sum_{k=0}^N \mathbf{1}^T \mathbf{y}(k) + \mathbf{c}_d^T \mathbf{d}(k) \right)}_{\text{revenue}} + \underbrace{\mathbf{c}_s^T \mathbf{z}}_{\text{storage investment}}$$

s.t.

$$(a) \quad \tilde{\mathbf{A}}_{\text{cost}}^x \mathbf{X} + \tilde{\mathbf{A}}_{\text{cost}}^y \mathbf{Y} \leq \tilde{\mathbf{b}}_{\text{cost}}$$

$$(b) \quad \tilde{\mathbf{A}}_{\text{in}}^g \mathbf{X} \geq \tilde{\mathbf{b}}_{\text{in}}^g$$

$$(c) \quad \tilde{\mathbf{A}}_{\text{eq}}^g \mathbf{X} = \tilde{\mathbf{b}}_{\text{eq}}^g$$

$$(d) \quad \mathbf{A}_s \begin{bmatrix} \mathbf{X} \\ \mathbf{z} \end{bmatrix} \leq \mathbf{b}_s$$

$$(e) \quad [\mathbf{A}_{\text{deg}}^u \mathbf{C}_s \quad \mathbf{A}_{\text{deg}}^z \quad \mathbf{A}_{\text{deg}}^D] \begin{bmatrix} \mathbf{X} \\ \mathbf{z} \\ \mathbf{D} \end{bmatrix} \leq \mathbf{b}_{\text{deg}}$$

$$(f) \quad \mathbf{X}_{\min} \leq \mathbf{X} \leq \mathbf{X}_{\max}, \quad (5)$$

where  $\mathbf{c}_s$  is the storage cost with respect to the horizon  $N$ ,  $\mathbf{c}_d$  specifies the storage cost and  $T$  is the sample interval. In contrast to our previous work, we also include battery degradation with  $\mathbf{D} = [\mathbf{d}(1), \dots, \mathbf{d}(N)] \in \mathbb{R}^{n_s \times 1}^T$  representing the capacity loss evolution. The overall objective consists of two parts: (1) storage investment and (2) revenue. It can be regarded as the total profit on the investment. The constraints of problem (5) are described in the following subsections.

1) *Generator cost functions (5a)*: Any convex cost structure of the operational domain can be considered by applying different cost data for the individual time steps:

$$\tilde{\mathbf{A}}_{\text{cost}}^x = \text{blkdiag}\{\mathbf{A}_{\text{cost},1}^x, \dots, \mathbf{A}_{\text{cost},N}^x\}, \quad (6)$$

$$\tilde{\mathbf{A}}_{\text{cost}}^y = \text{blkdiag}\{\mathbf{A}_{\text{cost},1}^y, \dots, \mathbf{A}_{\text{cost},N}^y\}, \quad (7)$$

$$\tilde{\mathbf{b}}_{\text{cost}} = [\mathbf{b}_{\text{cost},1}, \dots, \mathbf{b}_{\text{cost},N}]^T. \quad (8)$$

This generic representation allows us to model various tariff schemes such as high and low tariff schemes in combination with feed-in tariffs or even energy price profiles.

2) *Grid constraints (5b,c)*: To comply with the multi-period problem structure, the following matrices need to be accordingly replicated:

$$\tilde{\mathbf{A}}_g^{\text{in}} = \text{blkdiag}\{\mathbf{A}_{g,1}^{\text{in}}, \dots, \mathbf{A}_{g,N}^{\text{in}}\}, \quad (9)$$

$$\tilde{\mathbf{b}}_g^{\text{in}} = [\mathbf{b}_{g,1}^{\text{in}}, \dots, \mathbf{b}_{g,N}^{\text{in}}]^T, \quad (10)$$

$$\tilde{\mathbf{A}}_g^{\text{eq}} = \text{blkdiag}\{\mathbf{A}_{g,1}^{\text{eq}}, \dots, \mathbf{A}_{g,N}^{\text{eq}}\}, \quad (11)$$

$$\tilde{\mathbf{b}}_g^{\text{eq}} = [\mathbf{b}_{g,1}^{\text{eq}}, \dots, \mathbf{b}_{g,N}^{\text{eq}}]^T. \quad (12)$$

3) *Incorporation of Storage (5d)*: As specified in [12], we can describe the SoE evolution  $\mathbf{E}$  of  $n_s$  battery systems by

$$\mathbf{E} = \mathbf{S}_x \mathbf{e}(0) + \mathbf{S}_u \begin{bmatrix} \mathbf{p}_{\text{gen}}^{\text{s,dis}} \\ \mathbf{p}_{\text{gen}}^{\text{s,ch}} \\ \mathbf{p}_{\text{gen}}^{\text{eq}} \end{bmatrix}, \quad (13)$$

where  $\mathbf{S}_u \in \mathbb{R}^{n_s N \times 2n_s N}$ ,  $\mathbf{S}_x \in \mathbb{R}^{n_s N \times n_s}$  incorporate the storage dynamics and  $\mathbf{e}(0)$  denotes the initial SoE. The storage power variables for charging  $\mathbf{p}_{\text{gen}}^{\text{s,ch}} \in \mathbf{p}_{\text{gen}}$  and discharging  $\mathbf{p}_{\text{gen}}^{\text{s,dis}} \in \mathbf{p}_{\text{gen}}$  belong to the set  $\mathbf{x}$ . We can express  $\mathbf{E}$  with regard to  $\mathbf{x}$  and can specify the constraints by

$$\mathbf{A}_s = \begin{bmatrix} \mathbf{S}_u \mathbf{C}_s & [-\mathbf{1}^{N \times 1} \otimes \mathbf{I}^{n_s}] \\ -\mathbf{S}_u \mathbf{C}_s & \mathbf{0} \end{bmatrix}, \mathbf{b}_s = \begin{bmatrix} -\mathbf{S}_x \mathbf{e}(0) \\ \mathbf{S}_x \mathbf{e}(0) \end{bmatrix}, \quad (14)$$

where the matrix  $\mathbf{C}_s \in \mathbb{R}^{2n_s N \times 2n_l + 2n_g + n_b}$  assigns the storage power variables sequence to the optimization vector  $\mathbf{X}$ .

4) *Incorporation of Degradation (5e)*: Battery degradation reduces the available battery capacity. It has an impact on the overall profitability, since the storage revenue decreases over time due to the capacity loss. There is a complex relationship between battery degradation and operational management, such that the operational strategy has an impact on lifetime and profitability. From previous work [16] we use the concept of degradation maps that associate each discrete control action with an incremental capacity loss. By using a convex PWA representation of the degradation map it is possible to account for degradation in the operational domain with efficient optimization solvers. The PWA map for one battery system has the following structure

$$d = \max \left( \left[ \mathbf{a}_1 \quad \mathbf{a}_2 \quad \mathbf{a}_3 \right] \begin{bmatrix} p_{\text{bat}} \\ e \\ z \end{bmatrix} \right), \quad (15)$$

where  $\mathbf{a}_1, \mathbf{a}_2, \mathbf{a}_3$  are parameters that span planes in  $\mathbb{R}^3$ ,  $p_{\text{bat}}$  is the battery power and  $e$  denotes the battery's energy level. As an illustrative example, we show a degradation map for a LiFePO4 system in Fig. 3. The red surface represents an empirical degradation function from [17] that we have scaled and transformed to the energy/power domain. The blue PWA map denotes its convex hull that can be incorporated into efficient convex optimization solvers.

As described in [16] we can express the SoE evolution  $\mathbf{E}$  for multiple battery systems with respect to the storage power

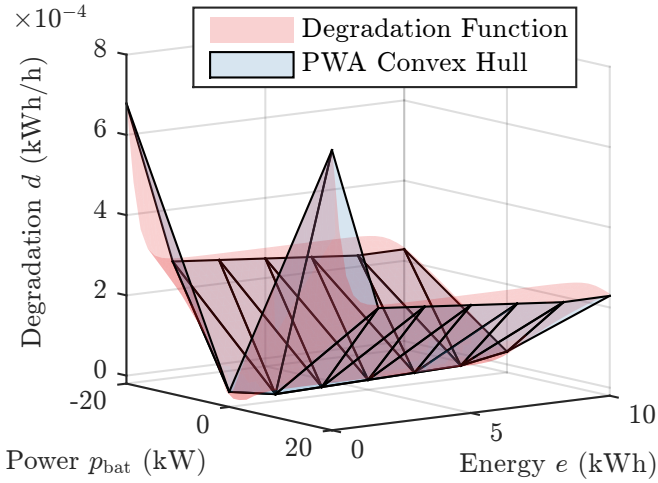


Figure 3. Illustration of a degradation map with an energy capacity of  $z = 10$  kWh. The red surface is the original degradation function from [17]. The blue piecewise-affine (PWA) map is its convex hull representation (15).

variables and obtain the following relations in order to include battery degradation in our placement and sizing problem:

$$\mathbf{A}_{\text{deg}}^u = [\mathbf{I}^{Nn_s} \otimes \mathbf{a}_1] [-\mathbf{I}^{Nn_s} - \mathbf{I}^{Nn_s}] + [\mathbf{I}^{Nn_s} \otimes \mathbf{a}_2] \mathbf{S}_u, \quad (16)$$

$$\mathbf{A}_{\text{deg}}^z = \mathbf{I}^N \otimes [\mathbf{I}^{n_s} \otimes \mathbf{a}_3], \quad (17)$$

$$\mathbf{A}_{\text{deg}}^D = \mathbf{I}^N \otimes -\mathbf{1}^{n_s \times 1}, \quad (18)$$

$$\mathbf{b}_{\text{deg}} = -[\mathbf{I}^{Nn_s} \otimes \mathbf{a}_2] \mathbf{S}_x. \quad (19)$$

### C. Benders Decomposition

Since the LP problem (5) is intractable for infinite prediction horizons, we try to decompose our placement and sizing problem. By exploiting the LP property, we can decompose our problem using Benders decomposition. We use the same decomposition procedure and notation according to [13].

1) *Master Problem*: According to [13] problem (5) has a decomposable structure, since  $z$  acts as the complicating variable. Hence, the problem can be split into a storage planning master problem and sequential-solvable subproblems reflecting the operational strategy. The master problem is

$$\begin{aligned} J^*(J_{\text{sub}}^{(l)}, \mathbf{z}^{(l)}, \boldsymbol{\lambda}_s^{(l)}) &= \min_{\mathbf{z}, \alpha} \mathbf{c}_s^T \mathbf{z} + \alpha \\ \text{s.t.} & \\ \text{(a)} \quad & J_{\text{sub}}^{(l)} + \boldsymbol{\lambda}_s^{T(l)} (\mathbf{z} - \mathbf{z}^{(l)}) \leq \alpha \\ \text{(b)} \quad & \alpha \geq \alpha_{\text{down}} \\ \text{(c)} \quad & \mathbf{0} \leq \mathbf{z} \leq \mathbf{z}_{\text{max}}, \end{aligned} \quad (20)$$

where  $l$  denotes the iteration of the master problem and  $\boldsymbol{\lambda}_s$  are the dual variables of  $z$  associated with the constraints of the subproblems. The variable  $J_{\text{sub}}$  denotes the sum of the subproblem objective values. Constraint (20a) represents the Benders cut at stage  $l$  and constraints (20b,c) specify the bounds of the optimization variables.

2) *Sequential Subproblems*: To reflect an MPC strategy we split the constraints in (5) with regard to the MPC prediction horizon  $H$  and to the partitions  $\mathbf{X} = [\mathbf{x}^{[1]}, \dots, \mathbf{x}^{[n]}]^T, \mathbf{Y} =$

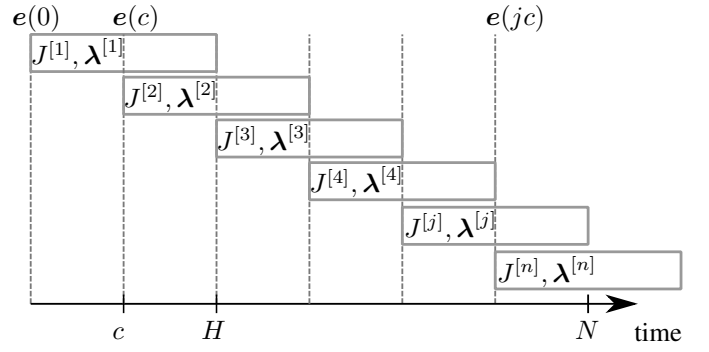


Figure 4. Sequence diagram of subproblem decomposition for a closed loop MPC strategy.

$[\mathbf{y}^{[1]}, \dots, \mathbf{y}^{[n]}]^T$ , and  $\mathbf{D} = [\mathbf{d}^{[1]}, \dots, \mathbf{d}^{[n]}]^T$  by defining  $\mathbf{A}^{[j]}, \mathbf{b}^{[j]}$ . The  $j$ -th coupled subproblem is defined as

$$\begin{aligned} J^{*[j]}(e(jc), \mathbf{z}) &= \min_{\mathbf{x}^{[j]}, \mathbf{y}^{[j]}, \mathbf{z}, \mathbf{d}^{[j]}} T \left( \sum_{k=0}^H \mathbf{1}^T \mathbf{y}^{[j]}(k) \right. \\ &\quad \left. + \mathbf{c}_d^{[j]T} \mathbf{d}^{[j]}(k) \right) \\ \text{s.t.} & \\ \text{(a)} \quad & \mathbf{A}^{[j]} \begin{bmatrix} \mathbf{x}^{[j]} \\ \mathbf{y}^{[j]} \\ \mathbf{z} \\ \mathbf{d}^{[j]} \end{bmatrix} \leq \mathbf{b}^{[j]}(e(jc)) \\ \text{(b)} \quad & \mathbf{z} = \mathbf{z}^{(l)} : \boldsymbol{\lambda}^{[j]}, \end{aligned} \quad (21)$$

where  $c$  denotes the update cycle of the subproblem recomputation. The coupling arises due to the fact that the actual SoE vector from the previous optimization cycle needs to be transferred to the consecutive subproblem as initial state input denoted by  $e(jc)$ . This fact does not allow us to solve the subproblems in a parallel fashion. The number of subproblems  $n$  depends on how often we rerun the optimization problems, which can be specified with the parameters  $c$  and  $N$ . We differentiate two cases that are described in the next subsections.

3) *Closed Loop - Receding Horizon MPC*: If  $c < H$  then the subproblems overlap. This is shown in Fig. 4, in which the control actions are applied to the system for  $c$  steps, before the next optimization problem is solved. This is also referred to as RHC and can be regarded as a closed loop feedback applied to the system. To account for this strategy, we need to assign the individual contribution of each subproblem within  $c$  steps in terms of the objective value and the dual variables  $\boldsymbol{\lambda}$ . This can be achieved by weighting  $\boldsymbol{\lambda}$  with

$$\boldsymbol{\lambda}_s = \sum_{j=0}^n \boldsymbol{\lambda}^{[j]} \frac{c}{H}, \quad (22)$$

and determining the total objective value (revenue) by

$$J_{\text{sub}} = \sum_{j=0}^n \sum_{k=0}^c \mathbf{1}^T \mathbf{y}_{\text{gen}}^{*[j]}(k) + \mathbf{c}_d^{[j]T} \mathbf{d}^{*[j]}(k), \quad (23)$$

where the total number of subproblems  $n$  that have to be solved is

$$n = \frac{N}{c}. \quad (24)$$

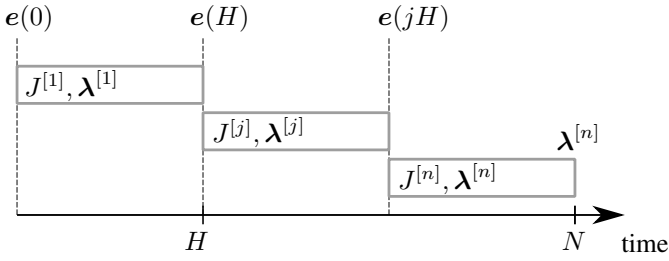


Figure 5. Sequence diagram of subproblem decomposition for an open loop MPC strategy.

4) *Open Loop MPC*: A special case of the general aforementioned case is the open loop case. In this case, the problems do not overlap any longer as depicted in Fig. 5, when  $c = H$ . By using this relation, Equations (22)-(24) are simplified to

$$\lambda_s = \sum_{j=0}^n \lambda^{[j]}, \quad J_{\text{sub}} = \sum_{j=0}^n J^{[j]}, \quad n = \frac{N}{H}. \quad (25)$$

5) *Algorithm*: With the aforementioned modifications we can solve the Benders decomposition in the same spirit as in [13]. The following Algorithm, Alg. 1, specifies the needed statements:

**Algorithm 1** Benders decomposition algorithm for optimal sizing and placement of distributed storage.

- 1:  $\mathbf{z} = \mathbf{0}$ ,  $\alpha_{\text{down}} = -100000$ ,  $l = 1$
- 2: solve master problem (20)  
 $[\mathbf{z}^{(l)}, \alpha^{(l)}] = \arg \min J^*$  discarding (20a)
- 3: **do**
- 4:   **if** ( $l > 1$ ) **then**
- 5:     calculate Benders cut (20a)
- 6:     solve master problem (20)  
 $[\mathbf{z}^{(l)}, \alpha^{(l)}] = \arg \min J^*(J_{\text{sub}}^{(l-1)}, \mathbf{z}^{(l-1)}, \lambda_s^{(l-1)})$
- 7:   **end if**
- 8:   **for**  $j = 0 : n$  **do**
- 9:     solve subproblem (21)  
 $[\mathbf{x}^{[j]}, \mathbf{z}, \mathbf{d}^{[j]}] = \arg \min J^{*[j]}(e(jc), \mathbf{z})$
- 10:   **end for**
- 11:   calculate  $\lambda_s$  with (22)
- 12:   calculate subproblem objective  $J_{\text{sub}}^{(l)}$  with (23)
- 13:    $Z_{\text{up}}^{(l)} = J_{\text{sub}}^{(l)} + \mathbf{c}_s^T \mathbf{z}^{(l)}$
- 14:    $Z_{\text{down}}^{(l)} = J_{\text{sub}}^{(l)} + \alpha^{(l)}$
- 15:    $l = l + 1$
- 16: **while**  $\left| \frac{Z_{\text{up}}^{(l)} - Z_{\text{down}}^{(l)}}{Z_{\text{down}}^{(l)}} \right| > \epsilon$

Note that the only difference from [13] is that we have to solve the subproblems in a sequential instead of a parallel fashion.

## IV. RESULTS

We aim to define a realistic case study that assesses the economic merit of different storage control strategies.

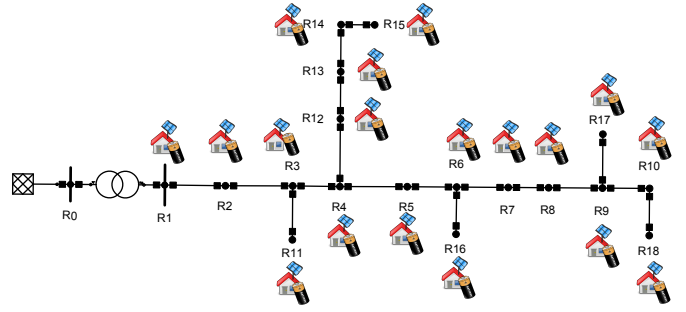


Figure 6. CIGRE test grid from [18] with a high PV infeed penetration.

Table I  
SIMULATION PARAMETERS.

Storage units	18
Storage power	$p_{\text{gen}}^{\text{s,max}} = 10\text{kW}$ , $q_{\text{gen}}^{\text{s,max}} = 10\text{kVar}$ , rect. bounded
Storage efficiency	$\eta_{\text{dis}} = 0.88$ , $\eta_{\text{ch}} = 0.88$
Degradation model	LiFePO4 convexified degradation map from [17]
Prediction horizon $H$	6, 12, 24 (1d), 168 (1w), 672 (1m)
Update cycle $c$	6
Sample time $T$	1h
Feed-in tariff $c_1^{\text{net}}$	50 €/MWh averaged from [20]
Net power cost $c_2^{\text{net}}$	246 €/MWh 6:00-22:00 (Mon-Sat) [19] 131.5 €/MWh rest of time
€ criterion	0.01
Battery cost $c_d$	50-1000 €/kWh
Investment cost $c_s$	5-100 €/(kWh a)
PV units	18
PV power	$p_{\text{gen}}^{\text{pv,max}} = 20\text{kW}$ , $q_{\text{gen}}^{\text{pv,max}} = 10\text{kVar}$ , rect. bounded
PV gen cost $c_1^{\text{pv}}$	0 €/MWh
Storage gen cost $c_1^{\text{s}}$	0 €/MWh
Total PV production	465 MWh
Total load consumption	61.5 MWh
Simulation horizon $N$	8760 (1 year)
Households	18 @ 4kW (randomized profile)
Grid	European LV network [18]
Voltage limits	$v_{\text{max}} = 1.1$ , $v_{\text{min}} = 0.9$
Thermal limits	according to [18]

### A. Test Case

As depicted in Fig. 6 we assume the LV CIGRE benchmark grid [18] as a realistic reference. As listed in Table I we configure the grid with a high PV penetration assuming that we can exploit the full roof top area of a single household. We compute the optimal locations and sizes of the batteries for different MPC controller strategies comprising different horizon lengths for a typical tariff scenario (day/night tariff [19] and feed-in tariff [20]) in Switzerland. We compute the placement and sizing problem for our scenarios on a one year base to include also the influence on seasonality, but also to save computation time. Therefore, we need to scale the investment battery cost with  $c_s$  accordingly to one year. In this regard we assume that the battery's calendar lifetime is at maximum 10 years.

### B. Heuristic Controller

To compare our enhanced predictive storage control strategy, we modify a standard heuristic control strategy that is described in [21]. In particular, we consider the storage control strategy that has a fixed feed-in limitation. This rule-based controller does not include any forecast of the PV production

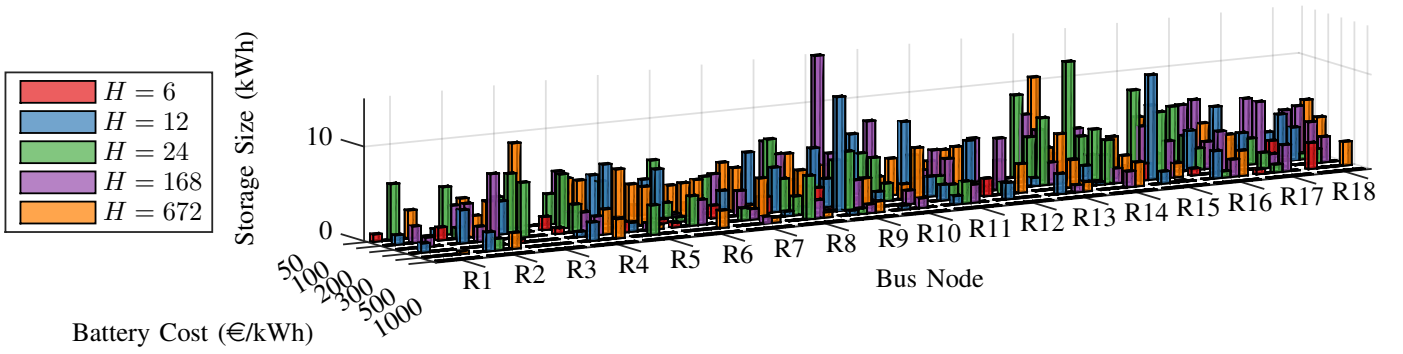


Figure 7. Optimal placement and sizes of the distributed battery storage as a function of the prediction horizon  $H$ , battery cost and bus nodes with reference to Fig. 6. Note that  $H$  specifies the horizon in discrete steps. Since the sample interval  $T$  is one hour,  $H$  corresponds also to hours in all figures.

and is therefore a non-predictive controller. It stores surplus PV power during the day and curtails PV power when the batteries are full and the grid limit is exceeded. In contrast to [21] and with the aim to utilize more PV power, we force to empty the batteries in the morning in case the available energy content was not consumed by the household over night. In addition, we determine dynamically the grid limits by running an AC Optimal Power Flow (AC-OPF). The AC-OPF framework allows us also to consider optimal RPC and APC.

Unfortunately, we cannot formulate an optimal placement and sizing problem using the proposed Benders decomposition technique, since this strategy does not provide any dual variables to reduce the space of feasible solutions by Benders cuts. However, to compare the strategies, we run the heuristic strategy with the optimal storage configuration that is obtained by the MPC strategy.

### C. Convergence and Computation Time

Figure 8 shows the typical convergence rate of our proposed Benders decomposition approach. One can observe that around 80 iterations are needed to reach the  $\epsilon$ -criterion specified in Alg. 1. The computation time ranges from 24 hours ( $H = 24$ ) to 3 days ( $H = 672$ ) to solve one scenario with the CPLEX LP solver [22]. Instead of solving each scenario consecutively, we run multiple scenarios in a parallel fashion on multi-core processors to save computation time.

### D. Sizing and Placement

First, we run the sizing and placement problem discarding the degradation model in the MPC strategy to further save computation time. Figure 7 shows the results of the storage placement and sizing problem as a function of different prediction horizons, battery costs and bus nodes of the benchmark grid. It can be observed that the biggest storage sizes are placed at the end of the branches such as R15, R14, and R9. This is comprehensible, since in this way network losses are reduced most effectively.

To draw concise conclusions, we further condense the results by presenting them in aggregated quantities. Figure 9 shows the aggregated placed storage size as a function of the battery cost. One can see that when decreasing the horizon length, less storage capacity is placed. In addition, at a cost

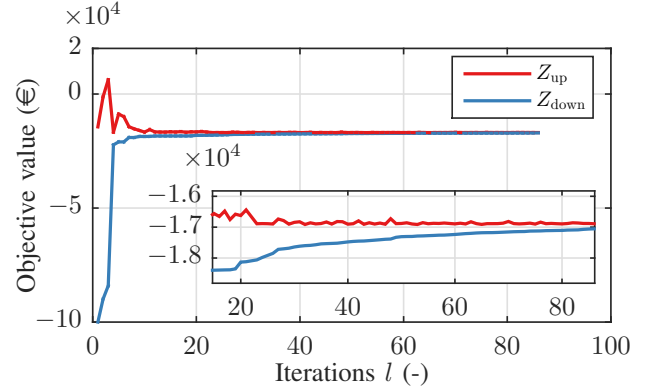


Figure 8. Typical convergence rate of the proposed Benders decomposition algorithm.

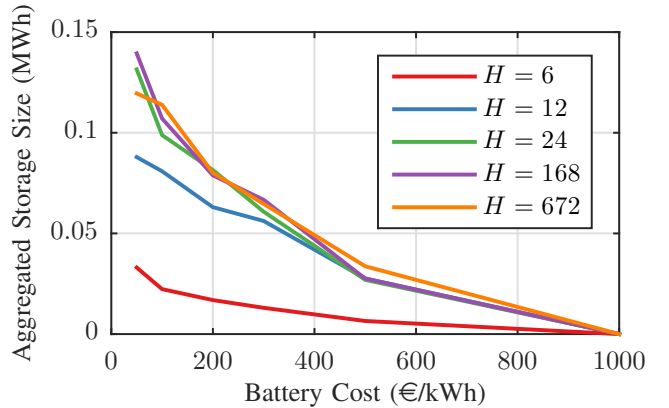


Figure 9. Aggregated storage size as a function of the battery cost for different prediction horizons.

level of 1000€/kWh it is not viable any longer to place storage in the grid. It is noteworthy that the storage size is almost the same, whether operating the storage in a daily ( $H = 24$ ), weekly ( $H = 168$ ) or monthly ( $H = 672$ ) fashion.

Fig. 10 shows the PV curtailment as a function of the battery cost for the different prediction horizons. One can observe that the curtailment levels are higher, when using sub-daily horizons. By using longer horizons (24, 168, 672) the PV curtailment is reduced by about half, since the aggregated storage size is higher for these controller strategies (see Fig. 9).

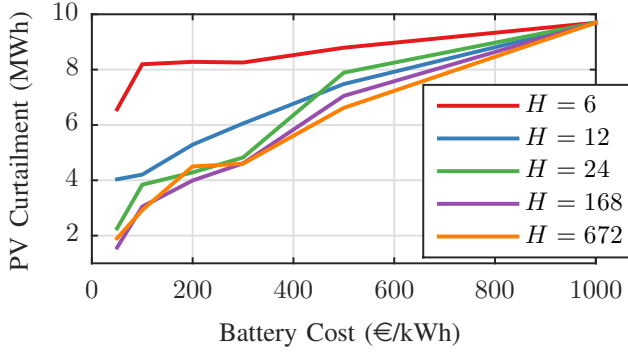


Figure 10. Total PV curtailment as a function of the battery cost for different prediction horizons.

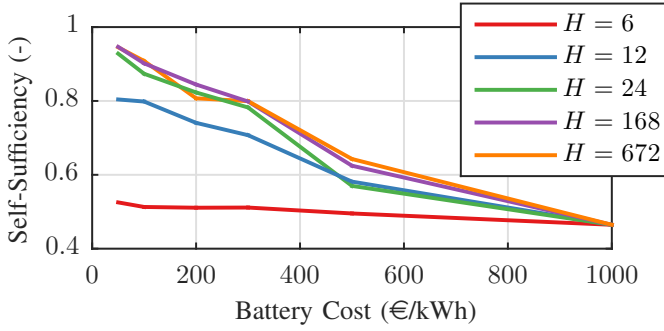


Figure 11. Self-sufficiency of the control area as a function of the battery cost for different prediction horizons.

However, despite of the same storage size, the degree of self-sufficiency of the control area for the horizon strategies (168,672) is in almost all cases higher (see Fig.11). This indicates that control strategies working on a weekly or monthly base are able to utilize more PV energy to cover the loads than in the case of much shorter daily cycles.

### E. Economic Value of Horizon Length

Next, we aim to compare the impact on the total investment profit for different prediction horizon lengths. Figure 12 shows the total investment profit as a function of the battery cost for different prediction horizons. One can observe that sub-daily horizon strategies are less profitable than daily, weekly or monthly horizon strategies. Another interesting result is that multi-day horizons perform rather equally, which means that longer prediction horizons than one day do not further improve the profit.

### F. Economic Assessment

For the economic assessment, we compare the MPC strategies with and without degradation model for a 24 hour horizon with the heuristic storage control strategy. By using the degradation map (15), we first compute the battery lifetime in  $m$  years for the different strategies according to the End of Life (EoL) criterion of 0.8. Here, the EoL defines the aggregated remaining capacity in the given control area after  $m$  years.

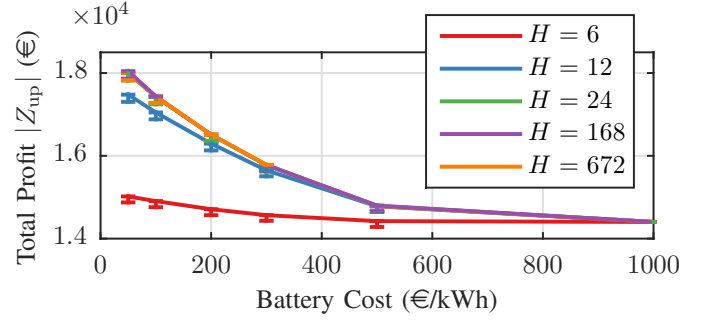


Figure 12. Total profit as a function of the battery cost for different prediction horizons considering a 1 year period.

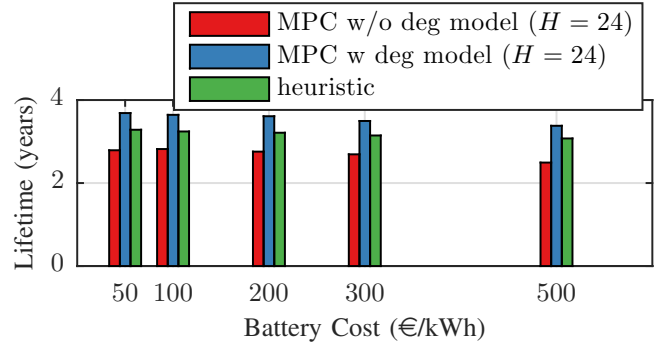


Figure 13. Battery lifetime as a function of the battery cost for different storage control strategies for an EoL criterion 0.8. Note that no battery capacity is installed for the battery cost of 1000€/kWh.

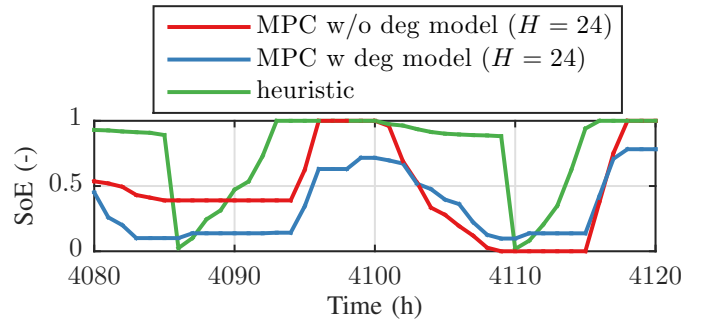


Figure 14. Resulting state of energy (SoE) trajectories from different storage control strategies.

This allows us to assume that the revenue streams over the years are approximately the same. Figure 13 shows the battery lifetimes for the different storage control strategies. It can be inferred that the storage control strategy has a great impact on battery lifetime. This can be explained by Fig. 14 that shows the resulting evolution of the SoE trajectories from the different controllers. While the MPC with degradation model avoids SoE regimes that are associated with high battery wear, the other ones idle the batteries at low SoE regimes or use the full capacity potential. The variable  $J_{\text{sub}}$  can be regarded as the revenue stream  $R$  for one year. To account only for the storage investment, we need to define the revenue difference considering an investment with (wS) and without storage

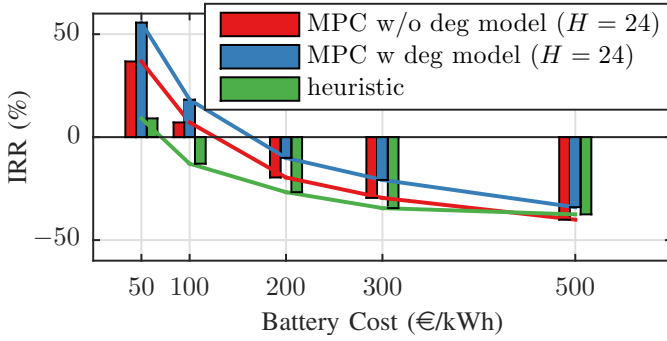


Figure 15. Internal Rate of Return (IRR) as a function of the battery cost for different storage control strategies.

(w/oS). The Net Present Value (NPV) of the investment is

$$\text{NPV} = -I_0 + \sum_{k=1}^m \frac{R_k^{wS} - R_k^{w/oS}}{(1 + \text{IRR})^k}, \quad (26)$$

$$= -c_d^T z + \sum_{k=1}^m \frac{-J_{\text{sub}}^{wS} + J_{\text{sub}}^{w/oS}}{(1 + \text{IRR})^k}, \quad (27)$$

where  $I_0$  is the storage investment. To obtain a viable investment the NPV has to be greater than zero. Since the Internal Rate of Return (IRR) is a direct measure for the ROI, we solve (27) for the IRR by setting the NPV to zero.

Although the lifetime is longer for the heuristic controller as compared to the MPC strategy without degradation model, the IRRs for the MPC strategies are superior, which are shown in Fig. 15. Below the battery cost of  $\approx 175\text{€/kWh}$  (w deg model) and  $\approx 125\text{€/kWh}$  (w/ deg model) the investments that use the MPC strategies are viable, while the heuristic strategy only achieves a profit below  $\approx 60\text{€/kWh}$ . This is due to the fact that the MPC strategies can generate more value by using forecasts and therefore better utilize the batteries.

## V. CONCLUSION

This paper presents a novel Benders decomposition method that considers MPC strategies in a planning problem. We split the sizing and placement problem into a master planning problem and sequentially-solvable subproblems reflecting a predictive storage control strategy. The storage control strategy is formulated as an MPC strategy that optimally schedules distributed battery storage to maximize PV self-sufficiency and PV utilization while considering grid constraints and minimizing battery degradation. The grid constraints are incorporated as a multi-period OPF problem using an existing linearized version of the OPF. Due to the linear property the placement and sizing problem can be decomposed by using Benders decomposition.

From the case study it can be concluded that MPC strategies are in general more profitable than heuristic controller strategies and are viable for battery cost below  $175\text{€/kWh}$ . The horizon length has a great impact on the profitability. Using prediction horizons that are shorter than 24 hours misses out substantial revenue potential, while using distributed battery storage on a daily base is as good as on a weekly or monthly

base in terms of the overall profit. Nevertheless, higher horizon lengths increase the self-sufficiency of the control area. It was shown that there exist optimal curtailment levels that depend on the battery cost. As a further finding, by using a battery degradation model within our MPC controllers, we can extend the battery lifetime and hence further increase the total profit.

## REFERENCES

- [1] F. J. de Sisternes, J. D. Jenkins, and A. Botterud, "The value of energy storage in decarbonizing the electricity sector," *Applied Energy*, vol. 175, pp. 368–379, 2016.
- [2] K. C. Divya and J. Ostergaard, "Battery energy storage technology for power systems - An overview," *Electric Power Systems Research*, vol. 79, no. 4, pp. 511–520, 2009.
- [3] B. Nykvist and M. n. Nilsson, "Rapidly falling costs of battery packs for electric vehicles," *Nature Climate Change*, vol. 5, no. 4, pp. 329–332, 2015.
- [4] R. Sims et al, *Integration of Renewable Energy into Present and Future Energy Systems*, ser. IPCC Special Report on Renewable Energy Sources and Climate Change Mitigation. Cambridge University Press, 2011.
- [5] N. Li, C. Uckun, E. M. Constantinescu, J. R. Birge, K. W. Hedman, and A. Botterud, "Flexible Operation of Batteries in Power System Scheduling with Renewable Energy," *IEEE Transactions on Sustainable Energy*, vol. 7, no. 2, pp. 685–696, 2016.
- [6] J. Eyer and G. Corey, "Energy Storage for the Electricity Grid : Benefits and Market Potential Assessment Guide," *SANDIA REPORT SAND2010-0815*, 2010.
- [7] P. Harsha and M. Dahleh, "Optimal sizing of energy storage for efficient integration of renewable energy," *IEEE Conference on Decision and Control and European Control Conference*, pp. 5813–5819, 2011.
- [8] —, "Optimal Management and Sizing of Energy Storage Under Dynamic Pricing for the Efficient Integration of Renewable Energy," *IEEE Transactions on Power Systems*, vol. 30, no. 3, pp. 1164–1181, 2014.
- [9] H. Pandzic, Y. Wang, T. Qiu, Y. Dvorkin, and D. S. Kirschen, "Near-Optimal Method for Siting and Sizing of Distributed Storage in a Transmission Network," *IEEE Transactions on Power Systems*, vol. PP, no. 99, pp. 1–13, 2014.
- [10] J. Weniger, T. Tjaden, and V. Quaschnig, "Sizing and grid integration of residential PV battery systems," *8th International Renewable Energy Storage Conference and Exhibition (IRES 2013)*, pp. 1–15, 2013.
- [11] Y. Yang, H. Li, A. Aichhorn, J. Zheng, and M. Greenleaf, "Sizing strategy of distributed battery storage system with high penetration of photovoltaic for voltage regulation and peak load shaving," *IEEE Transactions on Smart Grid*, vol. 5, no. 2, pp. 982–991, 2014.
- [12] P. Fortenbacher, M. Zellner, and G. Andersson, "Optimal sizing and placement of distributed storage in low voltage networks," in *19th Power Systems Computation Conference, Genoa, Italy*, 2016. [Online]. Available: <http://arxiv.org/abs/1512.01218>
- [13] A. Conejo, E. Castillo, R. Mínguez, and R. García-Bertrand, *Decomposition techniques in mathematical programming*, 2006.
- [14] L. Baringo and A. J. Conejo, "Wind power investment: A Benders decomposition approach," *IEEE Transactions on Power Systems*, vol. 27, no. 1, pp. 433–441, 2012.
- [15] P. Fortenbacher, J. Mathieu, and G. Andersson, "Optimal real-time control of multiple battery sets for power system applications," in *Proceedings of POWERTECH*, 2015.
- [16] P. Fortenbacher, J. L. Mathieu, and G. Andersson, "Modeling and Optimal Operation of Distributed Battery Storage in Low Voltage Grids," pp. 1–8, 2016. [Online]. Available: <http://arxiv.org/abs/1603.06468>
- [17] J. C. Forman, S. J. Moura, J. L. Stein, and H. K. Fathy, "Optimal Experimental Design for Modeling Battery Degradation," in *Proceedings of ASME Dynamic Systems and Control Conference*, vol. 1, 2012, pp. 309–318.
- [18] "Benchmark systems for network integration of renewable and distributed energy resources," Cigre Task Force C6.04.02, Tech. Rep., 2014. [Online]. Available: <http://c6.cigre.org/Publications/Technical-Brochures>
- [19] "Tariff scheme of the city Zurich for private households," Utility of the city Zurich, Zurich, Tech. Rep., 2016. [Online]. Available: <https://www.ewz.ch/content/dam/ewz/services/dokumentencenter/energie-beziehen/dokumente/gruener-strom-fuer-mein-zuhause/stromtarif-2016-zh-private.pdf>

- [20] "Feed in tariff of the city Zurich," Utility of the city Zurich, Zurich, Tech. Rep., 2016. [Online]. Available: <https://www.ewz.ch/content/dam/ewz/services/dokumentcenter/energie-produzieren/dokumente/verg{%}C3{%}BCtung-stromr{%}C3{%}BCcklieferung-2015-2016-zh.pdf>
- [21] J. Weniger, J. Bergner, and V. Quaschnig, "Integration of PV power and load forecasts into the operation of residential PV battery systems," *4th Solar Integration Workshop*, pp. 383–390, 2014.
- [22] "IBM ILOG CPLEX v12.1 user's manual for CPLEX," cplex, Tech. Rep., 2009. [Online]. Available: [ftp://public.dhe.ibm.com/software/websphere/ilog/docs/optimization/cplex/ps\\_usrmanplex.pdf](ftp://public.dhe.ibm.com/software/websphere/ilog/docs/optimization/cplex/ps_usrmanplex.pdf)